1 # Mantle earthquakes frozen in mylonitized ultramafic

2 # pseudotachylytes of spinel-lherzolite facies

3 **T. Ueda*[1], M. Obata[1], G. Di Toro[2], K. Kanagawa[3], K. Ozawa[4]**

4 **[[AU: Please give complete addresses (including cities and postal codes).]]**

5 *[1]Division of Earth and Planetary Sciences, Graduate School of Science, Kyoto University,*

6 *Japan*

7 *[2]Dipartimento di Geoscienze, Padova University, Italy*

8 *Istituto Nazionale di Geofisica e Vulcanologia, Rome, Italy*

9 *[3]Department of Earth Sciences, Chiba University, Japan*

10 *[4]Department of Earth and Planetary Sciences, Graduate School of Science, University of*

11 *Tokyo, Japan*

12 *E-mail: t_ueda@kueps.kyoto-u.ac.jp

13 **ABSTRACT**

14 We report a new type of ultramafic pseudotachylyte that forms a fault- and

15 injection-vein network hosted in the mantle-derived Balmuccia peridotite (Italy). In the

16 fault vein the pseudotachylyte is now deformed and recrystallized into a spinel-lherzolite

17 facies ultramylonite, made of a fine (<2 μm) aggregate of olivine, orthopyroxene,

18 clinopyroxene, and spinel, with small amounts of amphibole and dolomite. Electron

19 backscattered diffraction study of the ultramylonite shows a clear crystallographic

20 preferred orientation (CPO) of olivine. The fault vein pseudotachylyte overprints a

21 spinel-lherzolite facies amphibole-bearing mylonite, indicating that shear localization

22 accompanying chemical reaction had taken place in the peridotite before seismic slip

23   produced frictional melting. The occurrence of amphibole in the host mylonite and that of

24   dolomite as well as amphibole in the matrices of ultramylonite and pseudotachylyte may

25   indicate that fluid was present and had evolved in its composition from H_2O-rich to

26   CO_2-rich during ductile deformation with metamorphic reactions, which may account for

27   the observed rheological transition from ductile to brittle behavior. The spinel-lherzolite

28   facies assemblage in mylonites, *P-T* estimations from pyroxene geothermometry and

29   carbonate reactions, and the type of olivine CPO in deformed pseudotachylyte indicate that

30   both the preseismic and the postseismic ductile deformations occurred at ~800 °C and

31   0.7–1.1 GPa.

32   **Keywords:** pseudotachylyte, mantle, peridotite, mylonite, shear localization, earthquake,

33   fluid, dolomite, Balmuccia, Ivrea zone.

34   **INTRODUCTION**

35   Shear-induced rock melting during earthquakes may occur at mantle depths,

36   according to torsion experiments conducted under high confining pressure (Bridgman,

37   1936) and theoretical studies (e.g., Griggs and Handin, 1960). Kanamori et al. (1998)

38   assumed extensive production of seismic melts during the Mw = 8.3 Bolivian 1994

39   deep-focus (~600 km in depth) earthquake to justify its low seismic efficiency. The product

40   of solidification of seismic melts is pseudotachylyte, which allows us to study the

41   earthquake source mechanics complementary to the seismological one**[[AU: Wording?**

42   **(In particular, is the word "one" ambiguous?)]]** (e.g., Sibson, 1975; Di Toro et al.,

43   2005).

44   Ultramafic pseudotachylytes decorate exhumed faults cutting the subcontinental

45   peridotite lenses of Balmuccia (Obata and Karato, 1995) in Italy and the oceanic

46   peridotites in Corsica (Andersen and Austrheim, 2006). Common to these ultramafic

47   pseudotachylytes is the presence of microlites in a glassy matrix (Obata and Karato, 1995;

48   Andersen and Austrheim, 2006). In contrast to the ultramafic pseudotachylytes previously

49   described from the same (Obata and Karato, 1995) and other areas, this study shows

50   evidence for high-temperature mylonitization (in the spinel-lherzolite facies, ~800 °C) of

51   pseudotachylytes, among the highest ever reported. The sequence of events inferred from

52   structural and mineralogical observations supports the possibility of frictional melting and

53   will provide constraints on earthquake nucleation at mantle depths.

54   **GEOLOGIC SETTING**

55   The Balmuccia peridotite is a lenticular mass of spinel lherzolite of 5×0.8 km in

56   size, which is enclosed in an upper amphibolite to granulite facies mafic terrain—the Ivrea

57   zone, northern Italy (see Fig. 1 of Obata and Karato, 1995; the geologic map is also in the

58   GSA Data Repository Fig. DR1[1]). The main lithology of the peridotite massif is spinel

59   lherzolite and spinel harzburgite with porphyroclastic to granoblastic textures (e.g.,

60   Rivalenti et al., 1981; Sinigoi et al., 1983). Layers or dikes of pyroxenite are locally

61   abundant, some of which are folded and cut by faults associated with pseudotachylytes.

62   The peridotite was primarily equilibrated in the mantle at temperature and pressure

63   conditions of 1100 °C < T < 1200 °C and 1.3 GPa < P < 2.0 GPa, respectively (Shervais,

64   1979). Tectonic emplacement of the peridotite into the continental crust took place during

65   the Carboniferous at 300–320 Ma and was accompanied by high-grade metamorphism at

66   720 °C < T < 900 °C and 0.9 GPa < P < 1.1 GPa (Schmid and Wood, 1976; Handy et al.,

67   1999). The peridotite–mafic granulite complex was first exhumed during the Permian

68   transtension and the early Mesozoic rifting of the Piedmont Ligurian Ocean (Handy and

69   Stünitz, 2002) and then involved in the Tertiary brittle deformation along the Insubric Line

70   during the Alpine collision (Handy et al., 1999).

71   **HOST PERIDOTITES AND PSEUDOTACHYLYTES**

72   Pseudotachylytes, as commonly observed elsewhere (Sibson, 1975), occur as both

73   fault veins and injection veins, locally forming complex networks in the Balmuccia

74   peridotite. The pseudotachylyte fault veins are typically 1–10 mm thick, straight, and

75   appear black and glassy on fresh surfaces and light yellow on weathered surfaces (see

76   photos in Fig. DR2). At the banks along the Sesia River (45°49′12″N, 8°09′12″E), the fault

77   veins are subvertical and strike ~020° and 340°. The sense of shear and finite displacement

78   on these faults may sometimes be determined by the offset of the pyroxenite bands (Fig. 2

79   in Jin et al., 1998).

80   **Host Peridotites**

81   The host rock, away from fault veins, is protogranular coarse-grained spinel

82   lherzolite (with average modal composition, olivine [~60%], orthopyroxene [~25%],

83   clinopyroxene [~10%], and Cr-Al spinel [~5%]; Obata and Karato, 1995). Approaching

84   the fault, wall rocks are progressively deformed and recrystallized (Jin et al., 1998): They

85   form a protomylonite-mylonite consisting of plastically deformed porphyroclasts of

86   olivine, pyroxene, and spinel immersed in a fine-grained (10–50 μm) matrix of

87   recrystallized olivine, orthopyroxene, clinopyroxene, spinel, and pargasitic amphibole

88   (Fig. 1A). Within ~20 cm of the fault, the porphyroclasts are elongated and deflected

89   toward the fault (see a photomicrograph in Fig. DR3). Electron microprobe analyses show

90   that recrystallized neoblastic pyroxenes are distinctly less aluminous than the

91   porphyroclastic ones, while olivine is homogeneous (Fo_{89-90}) throughout (Table DR1, Fig.

92   DR4). The amphibole is titaniferous pargasite and typically occurs in fine-grained parts

93   (<60 μm, neoblasts) along grain boundaries of primary large crystals of olivine and

94   pyroxenes.

95   **Pseudotachylyte Fault (i.e., Ultramylonite) and Injection Veins**

96   The fault vein pseudotachylyte is foliated and mylonitized into a fine-grained (<2

97   μm) polymineralic matrix and is formally "ultramylonite" (Fig. 1A). The contact between

98   the wall rock mylonite and the ultramylonite is typically sharp because of the abrupt

99   reduction in grain size and the color contrast (the pseudotachylyte-derived ultramylonite

100   being more brownish in transmitted light; Fig. 1C). Some porphyroclasts in the host

101   mylonite are truncated by the ultramylonite fault vein (Fig. 1A). The ultramylonite

102   contains porphyroclasts of olivine, spinel, orthopyroxene, and clinopyroxene. The sense of

103   shear deduced from the δ-type porphyroclasts (e.g., dextral in Fig. 1B) in the fault vein is

104   consistent with that deduced from dike separations, with shape-preferred orientation (SPO)

105   in the ultramylonite matrix and with the deflection in the host mylonite.

106   The presence of an injection vein connected to the main ultramylonite shear band

107   (Fig. 1C; Fig. DR2) does suggest that the ultramylonite was originally a pseudotachylyte of

108   melt origin. While the main shear zone is foliated, the injection and the pockets are largely

109   massive but locally contain a weak foliation defined by the alignment of elongated olivine

110   clasts, subparallel to the injection wall and at high angles to the main fault vein.

111   Scanning electron microscope (SEM) investigations of the pseudotachylyte

112   revealed that both the fault and injection vein materials are holocrystalline, very

113   fine-grained (<2 μm) and equigranular to subequigranular, consisting of olivine,

114   orthopyroxene, clinopyroxene, and spinel, with small amounts (a few volume percent) of

115 amphibole and dolomite. Dolomite and amphibole were identified by a combination of

116 electron backscattered diffraction (EBSD) pattern and semiquantitative X-ray

117 spectroscopy. Dolomite is ubiquitous in the pseudotachylyte, both in the fault vein and in

118 the injection vein; it appears as dark phase in backscattered electron (BSE) images (Figs.

119 2A and 2B). An accurate modal amount of the amphibole is difficult to estimate in BSE

120 images but is probably less than a few percent according to EBSD analysis and

121 compositional mapping by X-ray spectroscopy. Olivine, pyroxene, amphibole, and

122 dolomite are texturally and thus chemically in equilibrium (Fig. 2A). In addition, the

123 injection veins contain numerous nanoparticles of Fe-Ni sulfide (as identified by

124 energy-dispersive X-ray spectroscopy [EDS])**[[AU: Can this be changed to**

125 **"energy-dispersive spectrometry [EDS]" or "energy-dispersive X-ray fluorescence**

126 **[EDS-XRF]" (per GSA style)?]]** along the grain boundaries, while the sulfide grains are

127 sparse and coarser-grained in the mylonitized fault vein. A shape-preferred orientation

128 (SPO) was observed in an injection vein at high magnification (Fig. 2A). The lack of

129 obvious SPO in the fault vein may be ascribed to more extensive recrystallization during

130 the postseismic shear. The SPO is subparallel to the wall of the injection vein and at high

131 angles to the fault vein. Furthermore, the fault vein has a clear crystallographic preferred

132 orientation (CPO) of olivine as described below.

133 **CRYSTALLOGRAPHIC PREFERRED ORIENTATION (CPO) OF OLIVINE**

134 Crystallographic orientations of olivine in the fault vein pseudotachylyte (i.e.,

135 ultramylonite) were studied using the EBSD technique. Measurements were made on a thin

136 section cut orthogonal to the fault foliation and parallel to the lineation, using a JEOL

137 JSM-6460 SEM (Chiba University) and a JEOL 7000F FE-SEM (University of Tokyo)

138   operating at 15–20 kV and 5–9 nA. Data were processed using HKL Channel-5 software

139   (Flamenco). Because of the small grain size (mostly less than 1 μm in diameter), indexing

140   of electron diffraction pattern together with phase identification was made manually on

141   each beam spot. The results are plotted in Figure 3.

142   Olivine exhibits a CPO with [100] axes subparallel to the lineation and [010] axes

143   subperpendicular to the foliation (Fig. 3) rather similar to the A-type fabric of Jung and

144   Karato (2001), which may indicate an activation of the (010)[100][[AU: OK? (As

145   opposed to "[010][100]" or "[010]-[100]"?)]] slip system in olivine (Carter and

146   Ave'Lallemant, 1970), suggesting a significantly high-temperature ductile deformation

147   within the fault vein.

148   The host, coarse-grained peridotite, remote from the fault vein, also has the A-type

149   CPO pattern, but with a distinct orientation of maxima from that of the mylonitized

150   pseudotachylyte (see Fig. 8 in Jin et al., 1998). The olivine CPO of protomylonite becomes

151   diffuse as the fault is approached, a result of the recrystallized fine-grained olivine having a

152   different CPO pattern from the porphyroclasts as seen in Figure 8B of Jin et al. (1998), i.e.,

153   a strong [001] maximum and diffuse [100] and [010] peaks. The latter is distinct from the

154   CPO we observed in the mylonitized pseudotachylyte.

155   **DISCUSSION**

156   **Sequence of Deformation and Crystallization Events**

157   From textural observation the sequence of events in the shear zone is inferred as

158   follows: (1) shear localization and recrystallization of host peridotite (that involve

159   hydration, i.e., the amphibole formation), producing a narrow mylonite zone, (2) a seismic

160   rupture and slip in or around the mylonite zone, which resulted in frictional melting and the

161   formation of pseudotachylyte, and (3) a further shear *within* the pseudotachylyte vein,

162   producing an ultramylonite. The deflection of the ultramylonite foliation at the mouth of

163   the injection vein (Fig. 1C) may indicate that flowing material was still hot and fluidal

164   during a residual shear of the main seismic slip and melting. The high-temperature CPO

165   (Fig. 3) is consistent with this inference. Petrological and mineralogical observations

166   indicate that this sequence of event took place under spinel-lherzolite facies conditions.

167   The preseismic ductile shear that produced the host mylonite was probably a slow

168   and long-lasting ductile deformation event, because the dominant mechanism of the

169   deformation is thought to be the dislocation creep coupled with metamorphic reactions,

170   which are governed by diffusive processes both in the solid and along grain boundaries.

171   Seismic rupture, on the other hand, involves rapid displacement (of the rate 1–5 m/s) and

172   rupture velocities (1–4 km/s; Scholz, 2002).

173   The observed transition from ductile shear to seismic rupture is puzzling because

174   ductile shear localization suggests strain softening (e.g., Jin et al., 1998), while seismic

175   rupture indicates a substantial stress accumulation. The association of pseudotachylyte and

176   mylonite has been observed in many localities (e.g., Sibson, 1980 **[[Q1: The in-text**

177   **citation "Sibson, 1980" is not in the reference list. Please correct the citation, add the**

178   **reference to the list, or delete the citation. Q1]]**; Passchier, 1982; White, 1996, 2004),

179   for which different interpretations have been proposed (e.g., Sibson, 1980 **[[Q2: The**

180   **in-text citation "Sibson, 1980" is not in the reference list. Please correct the citation,**

181   **add the reference to the list, or delete the citation. Q2]]**; Hobbs et al., 1986; White,

182   1996, 2004; Kelemen and Hirth, 2007). Because of the occurrence of amphibole in the

183   neoblasts in host mylonite and the ubiquity of dolomite in the pseudotachylyte, we infer

184   that fluid had evolved in composition during the preseismic ductile shearing and played an

185   important role in such a rheological transition.

186   **Fluid Chemistry Evolution and Consequences on Rock Strength**

187   We suppose that a fluid introduced in the shear zone originally contained CO_2 as

188   well as H_2O. The introduction of fluid and the progress of shear deformation may have

189   occurred concomitantly and cooperatively because metamorphic reactions and

190   recrystallization would enhance the rock ductility (e.g., White and Knipe, 1978). The

191   formation of amphibole in metamorphic reactions consumes H_2O, making the residual

192   fluid progressively enriched with CO_2 if the supply of a new fluid is limited or delayed.

193   The CO_2 enrichment in the fluid would reduce the connectivity of the fluid because of the

194   increase of fluid dihedral angle, thereby reducing the permeability (Watson and Brenan,

195   1987; Riley and Kohlstedt, 1990), thus impeding an external supply of additional H_2O-rich

196   fluid. The fluid-circulating system thus becomes unstable and will eventually become

197   closed due to the permeability loss. Once the system becomes closed, it will continue being

198   so until some catastrophic structural change such as rupture occurs. The ubiquity of

199   dolomite in the pseudotachylyte can suggest that the activity of H_2O was not internally

200   buffered during the preseismic metamorphism. The reduction of H_2O activity will cause a

201   hardening of olivine due to reduction of point defects (Karato et al., 1986). Thus the

202   reaction-controlled chemical evolution of the fluid from H_2O-rich to CO_2-rich likely

203   results in a strain hardening in the shear zone.

204   **Ambient Conditions During Deformation**

205   The temperature of the preseismic deformation was estimated to be ~800 °C by

206   applying the Ca-Mg exchange pyroxene geothermometer (Taylor, 1988) to the microprobe

207   analyses of the neoblastic pyroxenes in the host mylonite (Table DR1), and we consider

208   this representing the ambient condition of the seismic event. Given the grain size (<2 μm)

209   of the mylonitized pseudotachylyte vein, too small for microprobe analyses, we used the

210   dolomite-enstatite equilibria to estimate the *postseismic* ambient conditions. The

211   dolomite-enstatite stability field is bounded at high temperatures by the decarbonate

212   reaction (Fig. 4) (Brey et al., 1983),

213   enstatite + dolomite = diopside + forsterite + CO_2,   (1)
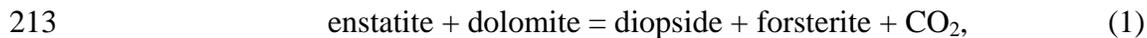
214   and at the low temperature by the reaction,

215   diopside + magnesite = enstatite + dolomite.   (2)

216   Note that reaction 2 is a CO_2-conserving reaction, and therefore it is independent of

217   the activity of CO_2. Considering the variability of the activities of H_2O and CO_2, it is

218   conceivable that the preseismic and postseismic recrystallizations share the same *P-T*

219   regime. It follows that pseudotachylyte were produced at ambient conditions of ~800 °C

220   and 0.7–1.1 GPa (Fig. 4). Given the exhumation history of the Balmuccia peridotite, this

221   *P-T* estimate would correspond to continental, lower-crust, or, probably (e.g., Fig. 11 in

222   Handy and Stünitz, 2002), upper-mantle deformation conditions.

223   **CONCLUSIONS**

224   Microstructural and mineralogical observations of an ultramafic mylonitized

225   pseudotachylyte have provided information about the seismic cycle at lower-crust or

226   upper-mantle conditions. The cycle includes initial fluid-assisted ductile shear localization

227   (producing host mylonite), followed by a seismic slip (producing pseudotachylyte), and

228   further ductile shear (producing ultramylonite). All these deformation events took place in

229   the spinel-lherzolite stability field (~800 °C and 0.7–1.1 GPa). Such high-temperature

230 deformation conditions preclude the formation or the preservation of glasses or quench

231 textures typically observed in more common shallow-seated pseudotachylytes, which

232 makes the recognition of pseudotachylytes difficult in high-grade terrains. Identification

233 and detailed study of such mylonitized pseudotachylytes remains an important task for

234 further study of earthquake mechanics in the upper mantle.

235 **ACKNOWLEDGMENTS**

246 **REFERENCES CITED**

247 Andersen, T.B., and Austrheim, H., 2006, Fossil earthquakes recorded by

248 pseudotachylytes in mantle peridotite from the Alpine subduction complex of Corsica:

249 Earth and Planetary Science Letters, v. 242, p. 58–72, doi:

250 10.1016/j.epsl.2005.11.058.

251   Brey, G., Brice, W.R., Ellis, D.J., Green, D.H., Harris, K.L., and Ryabchikov, I.D., 1983,

252   Pyroxene-carbonate reactions in the upper mantle: Earth and Planetary Science

253   Letters, v. 62, p. 63–74, doi: 10.1016/0012-821X(83)90071-7.

254   Bridgman, P.W., 1936, Shearing phenomena at high pressure of possible importance for

255   geology: Journal of Geology, v. 44, p. 653–669.

256   Carter, N.L., and Ave'Lallemant, H.G., 1970, High temperature flow of dunite and

257   peridotite: Geological Society of America Bulletin, v. 81, p. 2181–2202, doi:

258   10.1130/0016-7606(1970)81[2181:HTFODA]2.0.CO;2.

259   Di Toro, G., Nielsen, S., and Pennacchioni, G., 2005, Earthquake rupture dynamics frozen

260   in exhumed ancient faults: Nature, v. 436, p. 1009–1012, doi: 10.1038/nature03910.

261   Gasparik, T., 1984, Two-pyroxene thermobarometry with new experimental data in the

262   system CaO-MgO-Al_2O_3-SiO_2: Contributions to Mineralogy and Petrology, v. 87,

263   p. 87–97, doi: 10.1007/BF00371405.

264   Griggs, D., and Handin, J., 1960, Observations on fracture and a hypothesis of

265   earthquakes: Geological Society of America Memoir 79, p. 343–373.

266   Handy, M.R., and Stünitz, H., 2002, Strain localization by fracturing and reaction

267   weakening—A mechanism for initiating exhumation of subcontinental mantle

268   beneath rifted margins, *in* de Meer, S., et al., eds., Deformation mechanisms, rheology

269   and tectonics: Current status and future perspectives: The Geological Society of

270   London Special Publication 200, p. 387–407.

271   Handy, M.R., Franz, L., Heller, F., Janott, B., and Zurbriggen, R., 1999, Multistage

272   accretion and exhumation of the continental crust (Ivrea crustal section, Italy and

273   Switzerland): Tectonics, v. 18, p. 1154–1177, doi: 10.1029/1999TC900034.

274   Hobbs, B.E., Ord, A., and Teyssier, C., 1986, Earthquakes in the ductile regime?: Pure and

275   Applied Geophysics, v. 124, p. 309–335, doi: 10.1007/BF00875730.

276   Jin, D., Karato, S., and Obata, M., 1998, Mechanisms of shear localization in the

277   continental lithosphere: Inference from the deformation microstructures of peridotites

278   from the Ivrea zone, northwestern Italy: Journal of Structural Geology, v. 20,

279   p. 195–209, doi: 10.1016/S0191-8141(97)00059-X.

280   Jung, H., and Karato, S., 2001, Water-induced fabric transitions in olivine: Science, v. 293,

281   p. 1460–1463, doi: 10.1126/science.1062235.

282   Kanamori, H., Anderson, D.L., and Heaton, T.H., 1998, Frictional melting during the

283   rupture of the 1994 Bolivian earthquake: Science, v. 279, p. 839–842, doi:

284   10.1126/science.279.5352.839.

285   Karato, S., Paterson, M.S., and Fitz Gerald, J.D., 1986, Rheology of synthetic olivine

286   aggregates—Influence of grain size and water: Journal of Geophysical Research,

287   v. 91, p. 8151–8176, doi: 10.1029/JB091iB08p08151.

288   Kelemen, P.B., and Hirth, G., 2007, A periodic shear-heating mechanism for

289   intermediate-depth earthquakes in the mantle: Nature, v. 446, p. 787–790, doi:

290   10.1038/nature05717.

291   Obata, M., and Karato, S., 1995, Ultramafic pseudotachylite from the Balmuccia

292   peridotite, Ivrea-Verbano zone, northern Italy: Tectonophysics, v. 242, p. 313–328,

293   doi: 10.1016/0040-1951(94)00228-2.

294   Passchier, C.W., 1982, Pseudotachylyte and the development of ultramylonite bands in the

295   Saint-Barthelémy Massif, French Pyrenees: Journal of Structural Geology, v. 4,

296   p. 69–79, doi: 10.1016/0191-8141(82)90008-6.

297 Riley, G.N., Jr., and Kohlstedt, D.L., 1990, Melt migration in a silicate liquid-olivine

298 system: An experimental test of compaction theory: Geophysical Research Letters,

299 v. 17, no. 12, p. 2101–2104, doi: 10.1029/GL017i012p02101.

300 Rivalenti, G., Garuti, G., Rossi, A., Siena, F., and Sinigoi, S., 1981, Existence of different

301 peridotite types and of a layered igneous complex in the Ivrea zone of the western

302 Alps: Journal of Petrology, v. 22, p. 127–153.

303 Schmid, R., and Wood, B.J., 1976, Phase relationships in granulitic metapelites from the

304 Ivrea-Verbano zone (northern Italy): Contributions to Mineralogy and Petrology,

305 v. 54, p. 255–279, doi: 10.1007/BF00389407.

306 Scholz, C.H., 2002, The mechanics of earthquakes and faulting (2nd edition): Cambridge,

307 UK, Cambridge University Press, 471 p.

308 Shervais, J.W., 1979, Thermal emplacement model for the alpine lherzolite massif at

309 Balmuccia, Italy: Journal of Petrology, v. 20, p. 795–820.

310 Sibson, R.H., 1975, Generation of pseudotachylyte by ancient seismic faulting:

311 Geophysical Journal of the Royal Astronomical Society, v. 43, p. 775–794.

312 Sinigoi, S., Comin-Chiaramonti, P., Demarchi, G., and Siena, F., 1983, Differentiation of

313 partial melts in the mantle: Evidence from the Balmuccia peridotite, Italy:

314 Contributions to Mineralogy and Petrology, v. 82, p. 351–359, doi:

315 10.1007/BF00399712.

316 Taylor, W.R., 1988, An experimental test of some geothermometer and geobarometer

317 formulations: Neues Jahrbuch für Mineralogie, v. 172, p. 381–408.

318 Watson, E.B., and Brenan, J.M., 1987, Fluids in the lithosphere, 1: Experimentally

319 determined wetting characteristics of CO_2-H_2O fluids and their implications for fluid

320   transport, host-rock physical properties, and fluid inclusion formation: Earth and

321   Planetary Science Letters, v. 85, p. 497–515, doi: 10.1016/0012-821X(87)90144-0.

322   White, J.C., 1996, Transient discontinuities revisited: Pseudotachylyte, plastic instability

323   and the influence of low pore fluid pressure on deformation processes in the mid-crust:

324   Journal of Structural Geology, v. 18, p. 1471–1486.

325   White, J.C., 2004, Instability and localization of deformation in lower crust granulites,

326   Minas fault zone, Nova Scotia, Canada: The Geological Society of London Special

327   Publication 224, p. 25–37, doi: 10.1144/GSL.SP.2004.224.01.03.

328   White, S.H., and Knipe, R.J., 1978, Transformation- and reaction-enhanced ductility in

329   rocks: The Geological Society of London Journal, v. 135, p. 513–516.

330   **FIGURE CAPTIONS**

331   Figure 1. Optical images of the mylonitized pseudotachylyte. A: The wall rock

332   protomylonite (bottom) truncated by the ultramylonite (= mylonitized pseudotachylyte

333   fault vein, top). Cross-polarized light. B: Porphyroclastic system of spinel in the

334   mylonitized pseudotachylyte. The wings of stable spinel indicate high-temperature

335   deformation during postseismic deformation (see text). Fault plane is horizontal.

336   Plane-polarized light. C: Injection vein and pockets (black arrows) originated from

337   mylonitized pseudotachylyte fault vein. Pseudotachylyte pockets probably connected to

338   the fault vein, judging from observation of multiple thin sections of the same sample. Thin

339   white "ribbon" (white arrow) in the fault vein is elongated tail of clasts. Light-colored thick

340   bands labeled "Cl." are slices of host protomylonite. Red ellipse indicates the layer from

341   which CPO data (Fig. 3) were obtained. Sinistral shear. Plane-polarized light. Sample

342   VS14.

343

344   Figure 2. BSE image of an injection vein (A) and a fault vein pseudotachylyte (B) (sample

345   VS14) obtained at 15 keV. The direction of the fault plane is parallel to the short side of

346   photographs. Dol—dolomite; Sp—spinel; Sul—sulfide.

347

348   Figure 3. Pole figures of crystallographic orientations of olivine (axes [100], [010], and

349   [001]) in a mylonitized pseudotachylyte, obtained by EBSD. The data were obtained from

350   another thin section of the same sample (VS14); red ellipse in Figure 1C indicates the

351   relevant layer from which the EBSD data were obtained. Foliation is horizontal (XY plane,

352   solid line) with lineation (X). The shear sense is indicated by arrows on the top right.

353   Equal-area, lower-hemisphere projections. The gray shading is calculated with Gaussian

354   half-width of 15° referring to the density of data points (n = 164); the numbers in the legend

355   correspond to**[[AU: Should this be "are"?]]** the multiples of uniform distribution density.

356   A color version of the same diagram is given in Fig. DR4 (see footnote 1).

357

358   Figure 4. Ambient *P-T* condition for deformation of the wall rock (gray band) and of the

359   pseudotachylyte vein (area between thick lines; see text). Temperature obtained by

360   pyroxene geothermometer is indicated by a dashed line (the gray band includes the error).

361   Lherzolite facies boundaries (for $CaO-MgO-Al_2O_3-SiO_2$ system) after Gasparik (1984).

362   Reaction lines of carbonate (see text) after Brey et al. (1983). Di—diopside; En—enstatite;

363   Fo—forsterite.

364